THE JOURNAL OF BIOLOGICAL CHEMISTRY VOL. 284, NO. 39, pp. 26999–27009, September 25, 2009

Structural Plasticity of Malaria Dihydroorotate Dehydrogenase Allows Selective Binding of Diverse Chemical Scaffolds*[S]

Received for publication, June 1, 2009, and in revised form, July 8, 2009 Published, JBC Papers in Press, July 28, 2009, DOI 10.1074/jbc.M109.028589

Xiaoyi Deng[‡], Ramesh Gujjar[§], Farah El Mazouni[‡], Werner Kaminsky[§], Nicholas A. Malmquist[‡1], Elizabeth J. Goldsmith[¶], Pradipsinh K. Rathod[§2], and Margaret A. Phillips[‡3]

From the Departments of [‡]Pharmacology and [¶]Biochemistry, University of Texas Southwestern Medical Center at Dallas, Dallas, Texas 75390-9041 and the [§]Departments of Chemistry and Global Health, University of Washington, Seattle, Washington 98195

Malaria remains a major global health burden and current drug therapies are compromised by resistance. *Plasmodium falciparum* dihydroorotate dehydrogenase (*Pf*DHODH) was validated as a new drug target through the identification of potent and selective triazolopyrimidine-based DHODH inhibitors with anti-malarial activity *in vivo*. Here we report x-ray structure determination of *Pf*DHODH bound to three inhibitors from this series, representing the first of the enzyme bound to malaria specific inhibitors. We demonstrate that conformational flexibility results in an unexpected binding mode identifying a new hydrophobic pocket on the enzyme. Importantly this plasticity allows *Pf*DHODH to bind inhibitors from different chemical classes and to accommodate inhibitor modifications during lead optimization, increasing the value of *Pf*DHODH as a drug target. A second discovery, based on small molecule crystallography, is that the triazolopyrimidines populate a resonance form that promotes charge separation. These intrinsic dipoles allow formation of energetically favorable H-bond interactions with the enzyme. The importance of delocalization to binding affinity was supported by site-directed mutagenesis and the demonstration that triazolopyrimidine analogs that lack this intrinsic dipole are inactive. Finally, the *Pf*DHODH-triazolopyrimidine bound structures provide considerable new insight into species-selective inhibitor binding in this enzyme family. Together, these studies will directly impact efforts to exploit *Pf*DHODH for the development of anti-malarial chemotherapy.

The human malaria parasite is endemic in 87 countries putting 2.5 billion people in the poorest nations of the tropics at risk for the disease (1, 2). Despite intensive efforts to control malaria through combination drug therapy and insect control programs, malaria remains one of the largest global health problems. The most severe form of the disease is caused by *Plasmodium falciparum*, which kills 1–2 million people yearly, primarily children and pregnant woman. Effective vaccines have not been developed, and chemotherapy remains the mainstay of both treatment and prevention of the disease. Unfortunately widespread drug resistance to almost every known anti-malarial agent has compromised the effectiveness of malaria control programs (3). The introduction of artemisinin combination chemotherapy has provided new treatment options to combat drug-resistant parasites (4). However, recent reports by the World Health Organization suggest that resistance to artemisinin is developing along the Thai-Cambodian border, underscoring the need for a continual pipeline of new drug development to combat this disease.

The malaria parasite relies exclusively on *de novo* pyrimidine biosynthesis to supply precursors for DNA and RNA biosynthesis (5, 6). In contrast, the human host cells contain the enzymatic machinery for both *de novo* pyrimidine biosynthesis and for salvage of preformed pyrimidine bases and nucleosides. The lack of a redundant mechanism to acquire pyrimidines in malaria has raised interest in this pathway as a potential source for new therapeutic targets. Dihydroorotate dehydrogenase (DHODH)[4] is a flavin mononucleotide (FMN)-dependent mitochondrial enzyme that catalyzes the oxidation of dihydroorotate (DHO) to produce orotate, the fourth step in *de*

* This work was supported, in whole or in part, by National Institutes of Health Grants U01AI075594 and AI053680 (to M. A. P. and P. K. R.). This work was also supported by a grant from Malaria Medicines Venture (to M. A. P. and P. K. R.).

[S] The on-line version of this article (available at http://www.jbc.org) contains supplemental Table S1–S5 and Figs. S1–S4.

The atomic coordinates and structure factors (codes 3I65, 3I68, and 3I6R) have been deposited in the Protein Data Bank, Research Collaboratory for Structural Bioinformatics, Rutgers University, New Brunswick, NJ (http://www.rcsb.org/).

[1] Present address: Pasteur Institute, Paris 75724, France.

[2] Supported by a Senior Scholar Award in Global Infectious Diseases from the Ellison Medical Foundation and funds from the University of Washington Keck Center for Microbial Pathogens. To whom correspondence may be addressed. Tel.: 206-221-6069; E-mail: rathod@chem.washington.edu.

[3] Supported by Welch Foundation Grant I-1257 and the Carolyn R. Bacon Professorship in Medical Science and Education. To whom correspondence may be addressed: Dept. of Pharmacology, University of Texas Southwestern Medical Center at Dallas, 6001 Forest Park Rd., Dallas, TX 75390-9041. Tel.: 214-645-6164; E-mail: margaret.phillips@UTSouthwestern.edu.

[4] The abbreviations used are: DHODH, dihydroorotate dehydrogenase; *Pf*, *P. falciparum*; *h*, human; CoQ, coenzyme Q; FMN, flavin mononucleotide; DHO, dihydroorotate; A77 1726, 2-cyano-3-hydroxy-*N*-[4-(trifluoromethyl)-phenyl]-2-butenamide; brequinar, 6-fluoro-2-(2′-fluoro-1,1′-biphenyl-4-yl)-3-methyl-4-quinolinecarb oxylic acid; DSM1, 5-methyl-[1,2,4]triazolo[1,5-*a*]pyrimidin-7-yl)-naphthalen-2-yl-amine; DSM2, 5-methyl-[1,2,4]triazolo[1,5-*a*]pyrimidin-7-yl)-anthracen-2-yl-amine; DSM74, (5-methyl-[1,2,4]triazolo[1,5-*a*]pyrimidin-7-yl)-(4-trifluoromethyl-phenyl)-amine; DSM15, 5-methyl-7-(naphthalene-2-ylthio)-[1,2,4]triazolo[1,5-*a*]pyrimidine; DSM16, 5-methyl-7-(naphthalene-2-yloxy)-[1,2,4]triazolo[1,5-*a*]pyrimidine; *Pf*DHODH-DSM1, the x-ray structure of $PfDHODH_{\Delta 384-413}$ bound to DSM1; *Pf*DHODH-DSM2, the x-ray structure of $PfDHODH_{\Delta 384-413}$ bound to DSM2; *Pf*DHODH-DSM74, the x-ray structure of $PfDHODH_{\Delta 384-413}$ bound to DSM74; *Pf*DHODH-A77, the x-ray structure of *Pf*DHODH bound to A77 17267; *h*DHODH-bre, the x-ray structure of *h*DHODH bound to brequinar; *h*DHODH-A77, the x-ray structure of *h*DHODH bound to A77 1726; RMSD, root mean square deviation; SAR, structure activity relationship.

novo pyrimidine biosynthesis (7, 8). Coenzyme Q (CoQ) is required to catalyze the reoxidation of the flavin cofactor, and recent genetic studies suggest that the main function of mitochondrial electron transport in the parasite is to supply CoQ for this reaction (9). These studies provide genetic evidence that *Pf*DHODH is an essential enzyme to the malaria parasite. An inhibitor of human DHODH (*h*DHODH) (A77 1726 the active metabolite of leflunomide) is marketed for the treatment of rheumatoid arthritis, illustrating that DHODH is a druggable target (10, 11). Finally, biochemical (12, 13) and structural studies (14, 15) suggested that the identification of species-selective inhibitors against this target was feasible.

Our recent studies have since directly led to the validation of *Pf*DHODH as a new target for the discovery of anti-malarials. We utilized a high throughput screen to identify several classes of potent and species selective inhibitors of *Pf*DHODH (12, 16–18). These compounds are competitive with CoQ and inhibit the CoQ-dependent oxidation of FMN while not affecting the FMN-dependent oxidation of DHO. Site-directed mutagenesis data supported a model whereby the CoQ-binding site does not overlap with the inhibitor site, but instead inhibitors either block electron transfer between FMN and CoQ or stabilize a conformation that excludes CoQ binding (18, 19). Of the identified inhibitors, one promising series has emerged based on a triazolopyrimidine core structure (see Fig. 1 and Table 1). *Pf*DHODH inhibitors in this class show potent nanomolar activity against *P. falciparum in vitro*, with excellent correlation observed between inhibition of *Pf*DHODH and activity against the parasite (17, 18). We identified a metabolically stable derivative of this series (DSM74) that is able to suppress *Plasmodium berghei* infections in the malaria mouse model, providing the first proof that *Pf*DHODH inhibitors can have anti-malarial activity *in vivo* (17).

Interestingly, despite a vast number of ongoing attempts, *Pf*DHODH represents one of only a few truly new targets for the development of anti-malarial agents since the discovery that atovoquone targets the cytochrome bc_1 complex in the mitochondria (20). This has led to a substantial effort to target *Pf*DHODH for drug discovery programs and to the identification of diverse scaffolds showing species-selective inhibition of the enzyme (17, 18, 21–24). The prior structure of *Pf*DHODH complexed to A77 1726 (14), a *h*DHODH-specific inhibitor with poor affinity for *Pf*DHODH (19), neither explains the ability of *Pf*DHODH to bind the array of identified inhibitors nor provides an understanding of the developing SAR for the triazolopyrimidine-based inhibitor series.

Here we report the x-ray structures of *Pf*DHODH bound to three triazolopyrimidine-based inhibitors with different sized substituents bound to the triazolopyrimidine core. In addition, we examined the small molecule x-ray structures of these inhibitors and compared them with the protein-bound ligand structures. Finally, the inhibitor-bound *Pf*DHODH structures were compared with the structures of *h*DHODH bound to A77 1726 and to brequinar, a potent 4-quinolinecarboxylic acid inhibitor of the human enzyme (25, 26). Together these studies explain both the high affinity binding and species selectivity of this important class of *Pf*DHODH inhibitors, thus laying the foundation for future lead optimization programs for the present anti-malarial agents. More broadly, this study provides new, unexpected insight into why *Pf*DHODH is a highly attractive drug target for a large set of diverse chemical entities with potential for sustainable, robust lead optimization programs.

EXPERIMENTAL PROCEDURES

Gene Cloning of PfDHODH—N-terminally truncated *Pf*DHODH (amino acids 159–569) was PCR-amplified with primers 1 (5′-AAGGATCCGTTTGAATCTTATAACCCG-3′) and 4 (5′-GGGTCGACTTCCATGGTACCAGCTGCAG-3′) from plasmid pRSET-pfDHODH encoding the codon optimized gene (provided by Jon Clardy) (14) and ligated into the pET28b (Novagen) expression vector at the BamH1/SalI sites. $PfDHODH_{\Delta 384-413}$ was generated by PCR amplification of two fragments with compatible restriction sites that excluded the loop sequence. Fragment 1 (amino acids 159–383) containing 5′-BamHI and 3′-EcoRI was generated using primers 1 and 2 (5′-GGGAATTCGTCATTCATAATGTTATTTT-3′) and fragment 2 (amino acids 414–569) containing 5′-EcoRI and 3′-SalI was PCR-amplified with primers 3 (5′-GGGAATTCCTGTGGTTTAATACCACGAA-3′) and 4. Both PCR products were subcloned separately into pCR-Blunt II-TOPO vector (Invitrogen). The resulting clones were used to generate the final expression clone containing loop-truncated $PfDHODH_{\Delta 384-413}$ in pET28b in frame with an N-terminal His_6 tag.

Protein Expression and Purification—Escherichia coli BL21 phage-resistant cells (Novagen) were used for the expression of pET28b wild-type *Pf*DHODH and $PfDHODH_{\Delta 384-413}$ constructs using a modification of methods described previously (19). Proteins were expressed in Terrific Broth medium containing kanamycin (50 μg/ml). The cells were grown to 0.8 A_{600} at 37 °C, 0.2 mM isopropyl-β-D-thiogalactoside was added to induce protein expression, and the cells were grown overnight at 16 °C. The cells were pelleted by centrifugation (4000 × *g*) and resuspended in lysis buffer (100 mM HEPES, pH 8.0, 150 mM NaCl, 10% glycerol, and 0.05% THESIT detergent (Fluka)), containing protease-inhibitor mixture for His tag protein (Sigma). The cells were lysed by three passes through an Emulsi-Flex-C5 high pressure homogenizer (Avestin Inc.), the lysate was clarified by centrifugation (20,000 × *g*), and the resulting supernatant was applied to a HisTrap HP column (GE Healthcare) precharged with Ni^{+2}. The column was sequentially washed with lysis buffer and lysis buffer containing 20 mM imidazole. *Pf*DHODHs were eluted from the column using a linear gradient from 20 to 400 mM imidazole. Fractions containing *Pf*DHODH were pooled, concentrated with Amicon Ultra concentrator (Millipore), and then purified by gel filtration column chromatography on a HiLoad 16/60 Superdex 200 column (GE Healthcare) equilibrated with crystallization buffer (10 mM HEPES, pH 7.8, 100 mM NaCl, 1 mM *N*,*N*-dimethyldodecylamine *N*-oxide (Fluka), 5% glycerol, 10 mM dithiothreitol). Fractions containing *Pf*DHODH were pooled and concentrated to 20 mg/ml. The construction and purification of the H185A, F188A, F227A, and R265A mutant *Pf*DHODH enzymes were described previously (12, 19).

Enzyme Kinetic Analysis—Steady-state kinetic analysis was performed as described previously (12, 19). To determine the

k_{cat} and K_m of *Pf*DHODH$_{\Delta 384-413}$ in comparison with the wild-type enzyme the direct assay that follows the oxidation of DHO at 296 nM ($\epsilon = 4.3$ mM^{-1} cm^{-1}) was used (Supplemental Table S1). The reactions were performed in assay buffer (100 mM HEPES, pH 8.0, 150 mM NaCl, 10% glycerol, 0.1% Triton) at 20 °C for a range of CoQ_D (0.025–0.15 mM) and DHO concentrations (0.01–0.5 mM) with *Pf*DHODH (2 nM). Inhibitor kinetics for both wild-type (10 nM) and mutant (10 nM) *Pf*DHODH were followed using the indirect assay that couples the oxidation of DHO (0.2 mM) in the presence of CoQ_D (20 μM) to the reduction 2,6-dichloroindophenol (60 μM) at 600 nM ($\epsilon = 18.8$ mM^{-1} cm^{-1}). The data were fitted to the Michaelis-Menten equation to determine the steady-state kinetic parameters or to the following equation to determine the IC_{50} values using Graph Pad Prism (Graph Pad), v_i = Bottom + (Top − Bottom)/(1 + $10^{(\mathrm{Log[I]-LogIC50})}$), where, v_i is the initial velocity (s^{-1}), and Top and Bottom represent the plateaus in velocity units.

Crystallization and Data Collection of PfDHODH$_{\Delta 384-413}$ Bound to Inhibitors—Random crystallization screen *Cryo* suite (Nextal) and detergent screen kits (Hampton Research) were utilized to determine preliminary crystallization conditions. Subsequent refinement of pH, precipitant, detergent, and protein concentrations was then done to find optimal conditions. *N*,*N*-Dimethyldodecylamine *N*-oxide (1 mM) was found to improve crystallization, and it was subsequently added during the final gel filtration purification step. The crystals of *Pf*DHODH$_{\Delta 384-413}$ were grown by vapor diffusion in hanging drop at 20 °C. Reservoir solution (0.16 M ammonium sulfate, 0.1 M sodium acetate, pH 4.6, 18–20% polyethylene glycol 4000, 25% glycerol, and 10 mM dithiothreitol) was mixed with an equal volume of *Pf*DHODH$_{\Delta 384-413}$ (15 mg/ml) containing inhibitor (DMS1 (0.6 mM); DSM2 (0.6 mM), or DSM74 (1 mM)) and DHO (2 mM). The crystals typically grew in 4–7 days.

Diffraction data were collected at 100 K on Beamline 19ID at Advanced Photon Source using an ADSC Q315 detector. *Pf*DHODH-DSM1 diffracted to 2.0 Å and has a space group of $P6_4$ with the cell dimension of $a = b = 85.9$, $c = 138.4$; *Pf*DHODH-DSM2 diffracted to 2.4 Å with space group $P6_4$ and cell dimension of $a = b = 85.9$, $c = 138.7$; and *Pf*DHODH-DSM74 diffracted to 2.7 Å with space group $P6_4$ and cell dimension of $a = b = 85.4$, $c = 138.6$ (supplemental Table S2). All three structures have one molecule of *Pf*DHODH in the asymmetric unit. Diffraction data were integrated, and intensities were scaled with the HKL2000 package (27).

Structure Determination and Refinement of PfDHODH Bound to Inhibitors—Crystallographic phases for *Pf*DHODH-DSM1 were solved by molecular replacement with Phaser (28) using the previously reported structure of *Pf*DHODH bound to A77 1726 (Protein Data Bank code 1tv5) (14) as a search model. *Pf*DHODH-DSM1 was used as the search model to find solutions for *Pf*DHODH-DSM2 and *Pf*DHODH-DSM74. Structures were rebuilt with COOT (29) and refined with REFMAC (30), and phases were improved with DM (31) (supplemental Table S2). All of the residues were within the allowed section of the Ramachandran plot (supplemental Table S2). Water molecules were added if the density was stronger than 3.4 σ and removed if the density was weaker than 1 σ in the density map with ARP/warp (32). For *Pf*DHODH-DSM1 the final structure contains residues Ser^{160}–Ser^{567}, with the exception that density was not observed for a loop formed by residues 348–355, 124 water molecules, and a bound LDHO detergent molecule. The final DSM2- and DSM74-bound *Pf*DHODH structures contain all residues between Glu^{159}–His^{566} (*Pf*DHODH-DSM2) and Phe^{161}–His^{566} (*Pf*DHODH-DSM74), plus 63 and 38 water molecules, respectively. No density was observed for the detergent molecule in these structures. In the DSM1-, DSM2-, and DSM74-bound structures the shortened surface loop at position 384 is observed in its entirety.

Molecular Modeling—The structures were displayed using the graphics program PyMol (26). The *Pf*DHODH-DSM1 structure was superimposed with the *Pf*DHODH-DSM2, *Pf*DHODH-DSM74, *Pf*DHODH-A77 (Protein Data Bank code 1tv5), *h*DHODH-A77 (Protein Data Bank code 1D3H) (15), and *h*DHODH-bre (Protein Data Bank code 1D3G) (15) structures by aligning only backbone atoms of the β/α domain in LSQKAB (33). For the alignment between *pf*DHODH-DSM1 and *h*DHODH, the following sequences were superimposed: *Pf* 217–232 to *h*88–103; *Pf*271–278 to *h*142–149; *Pf*337–343 to *h*207–213; *Pf*436–460 to *h*262–286; *Pf*473–494 to *h*301–322; *Pf*501–529 to *h*329–357; and *Pf*541–552 to *h*369–380. The same *Pf*DHODH residues were used to superimpose the various *Pf*DHODH structures. RMSD values were calculated for the superimposed structures based on the C_α positions using LSQMAN (32, 34). Moleman2 (35) was used to manipulate the Protein Data Bank files before the analysis (Software was obtained from the Uppsala Software Factory.).

Small Molecule X-ray Structure Determination—Crystallization of DSM1 from CH_2Cl_2/CH_3OH was described previously (18). DSM15, DSM16, and DSM74 were crystallized similarly to CH_2Cl_2. Single crystals were mounted on a glass capillary with oil. The data were collected at −143 °C with a Nonius Kappa CCD FR590 single crystal x-ray diffractometer. The crystal-to-detector distance was 30 mm. Other data collection parameters are summarized in supplemental Table S3. The data were integrated and scaled using hkl-SCALEPACK (27). Solution by direct methods (SIR97) (36) produced a complete heavy atom phasing model (supplemental Table S4). All of the hydrogen atoms were located using a riding model with the exception of H1. All of the non-hydrogen atoms were refined anisotropically by full matrix least squares utilizing SHELXL97 (37). Scattering factors are from Waasmaier and Kirfel (38), and the absolute structure assignment for DSM1 was established via anomalous scattering. The Flack enantiopole parameter (39) is −0.06 ± 0.11. ORTEP drawings (40) are shown in supplemental Fig. S4.

The crystals of DSM15 were twinned such that two lattices of very similar intensities were apparent in the diffraction pattern. One lattice was indexed. In a first refinement cycle, intensities of reflections of type {0 k l} (10% of total data) appeared systematically larger than those calculated. Excluding {0 k l} reflections from the refinement allowed a useful structure to be determined. The ratio between the calculated and measured intensities of the excluded data was close to 2, consistent with a total overlap of two data sets. Such twining can arise from 2-fold twinning along [1 0 0] or a mirror on the [0 k l] plane. No additional twin law was found for the reduced data set, indicating that the twinning did not create any detectable intensity

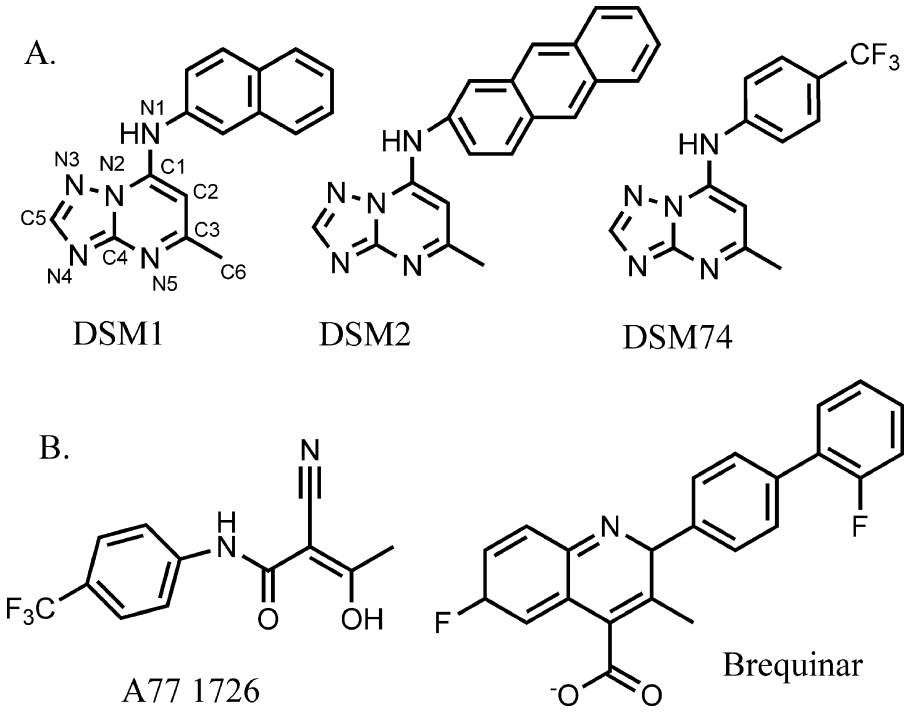

FIGURE 1. **Inhibitors of dihydroorotate dehydrogenase.** *A*, selective inhibitors of *Pf*DHODH. DSM1, DSM2, and DSM74. *B*, selective inhibitors of human DHODH, A77 1726, and brequinar.

overlaps for other peaks. Thus the excluded intensity data were corrected for the factor 2 and merged with the other data for the final structural refinement.

For DSM74 some of the intermolecular fluoride-fluoride distances were too short. This problem arises from disorder of the CF_3 group. CF_3 groups are very often found to rotate or be arranged in two alternating geometries. This is the case in this structure where two conformations of the CF_3 (atoms F1–3 and F4–6) were refined at half-site occupancies including the carbon. However the disorder, which is represented by to a 2-fold rotation around the axis C7-N1, extended to the phenyl group, which is also represented in the refinement by two rings of half-site occupancies. When F1 (F4) is present, the symmetry related F2 (F5) of the same disordered moiety is absent, which, if there were no defects or additional voids in the crystal, would require a structure with the disordered CF_3 alternating, which in turn would cause a doubled *c* axis length. There is evidence in the scattering for this to be partially the case because there are very faint reflections in the diffraction images pointing toward a doubled *c* axis; however, the order is not persistent throughout the whole crystal. The disorder required a special refinement where the phenyl ring was constrained in its angles, but the average distance between the atoms was freely refined. The distances of the disordered rings to the neighboring atoms are as follows: N-1–C-7, 1.42 ± 0.02; N-1–C-7′, 1.44 ± 0.02; C-10–C-13, 1.50 ± 0.02; and C-10′–C-13′, 1.51 ± 0.02.

Synthetic Methods: General Chemistry and Analysis—The reagents and solvents were obtained from commercial suppliers and were used without further purification. The reaction progress was monitored by TLC using silica gel 60 F-254 (0.25 mm) plates and detection with UV light. Flash chromatography was carried out with silica gel (32–63 μm). ^{1}H NMR spectra were recorded in $CDCl_3$ at 300 MHz. Chemical shifts are reported in parts per million (δ) downfield from tetramethylsilane. Coupling constants (*J*) are reported in Hz. Spin multiplicities are described as s (singlet), brs (broad singlet), d (doublet), t (triplet), q (quartet), and m (multiplet). Electrospray ionization mass spectra were acquired on a Bruker Esquire liquid chromatograph ion trap mass spectrometer. Melting points (Pyrex capillary) were determined on a Mel-Temp apparatus and are uncorrected.

DSM1, DSM2, and DSM74 were prepared as described previously (17, 18). DSM15 and DSM16 were prepared as shown in supplemental Fig. S3. Condensation of 3-amino-[1,2,4]triazole with ethyl acetoacetate in acetic acid yielded the 7-hydroxy-[1,2,4]-triazolo[1,5-*a*]pyrimidine. Chlorination with phosphorous oxychloride gave the corresponding 7-chloro-[1,2,4]triazolo[1,5-*a*]pyrimidine as described previously (18), which upon treatment with 2-thionaphthol/2-naphthol (1.2 eq) in 5 ml of DMF, K_2CO_3 (1.2 eq) stirred under N_2 atmosphere at room temperature for a 20-h yielded product. The crude products were purified by column chromatography using ethyl acetate/hexane.

Physical Properties—The physical properties are as follow: 5-methyl-7-(naphthalene-2-ylthio)-[1,2,4]triazolo[1,5-*a*]pyrimidine (DSM15), mp 189 °C; ^{1}H NMR (300 MHz, $CDCl_3$): δ 8.50 (s, 1H), 8.30 (s, 1H), 8.10–7.94 (m, 3H), 7.74–7.62 (m, 3H), 6.16 (s, 1H), 2.48 (s, 3H); MS *m/z* 293.1 $[M + H]^+$; and 5-methyl-7-(naphthalene-2-yloxy)-[1,2,4]triazolo[1,5-*a*]pyrimidine (DSM16); mp 170 °C; ^{1}H NMR (300 MHz, $CDCl_3$): δ 8.51 (s, 1H), 8.05 (d, J = 9 Hz, 1H), 8.01–7.88 (m, 2H), 7.78 (m, 1H), 7.68–7.58 (m, 2H), 7.45–7.38 (m, 1H), 6.08 (s, 1H), 2.58 (s, 3H). MS *m/z* 277.2 $[M + H]^+$.

RESULTS

X-ray Structure Determination of PfDHODH Bound to Triazolopyrimidine Analogs—Three triazolopyrimidine analogs containing naphthyl (DSM1), anthracenyl (DSM2), and phenyl-trifluoromethyl (DSM74) substituents, which span a range of inhibitor potency (0.05–0.3 μM), were chosen for crystallographic analysis (Fig. 1 and Table 1). Proteolysis of a *P. falciparum*-specific surface loop, which is not present in the enzymes from human or other *Plasmodium* species (residues 384–413; Fig. 2), led to difficulties obtaining diffraction quality crystals with these inhibitors. To improve crystallization we generated a *Pf*DHODH construct lacking amino acid residues 384–413 ($PfDHODH_{\Delta 384-413}$). This region of the structure was missing or disordered in the *Pf*DHODH structure described previously (14). Steady-state kinetic analysis of $PfDHODH_{\Delta 384-413}$ demonstrated

that the catalytic efficiency and inhibitor binding properties of the loop-minus protein were similar to the wild-type enzyme (supplemental Table S1). *Pf*DHODH$_{\Delta 384-413}$ was co-crystallized with DSM1, DSM2, or DSM74 in the presence of substrate DHO, and 2.0, 2.4, and 2.7 Å resolution data sets were collected, respectively. The three structures were solved by molecular replacement and refined to R_{fac} of 23.1, 22.5, and 23.6 and R_{free} of 24.8, 26.7, and 27.6, respectively (supplemental Table S2).

TABLE 1

Inhibition kinetics of wild-type and mutant *Pf*DHODH

The error represents the standard error of the mean for $n = 4-5$. The fold change is shown in parentheses. The IC_{50} values for A77 1726 against *Pf*DHODH and *h*DHODH are 180 μM (19) and 0.3–1 μM (54–56), respectively. Brequinar binds *h*DHODH with an IC_{50} of 0.006–0.01 μM (54–56).

Inhibitor enzyme	IC_{50}		
	DSM1	DSM2	DSM74
		μM	
*Pf*DHODH	0.047[a]	0.056[a]	0.28[b]
*h*DHODH	>100[a]	>100[a]	>100[b]
*Pf*DHODH-H185A	1.3 ± 0.17 (28)	1.3 ± 0.17 (23)	25 ± 9.0 (90)
*Pf*DHODH-R265A	2.1 ± 0.70 (45)	2.4 ± 1.1 (43)	23 ± 6.7 (82)
*Pf*DHODH-F227A	1.3 ± 0.086 (28)	4.4 ± 1.1 (79)	6.3 ± 1.1 (23)
*Pf*DHODH-F188A	2.1 ± 1.4 (45)	0.21 ± 0.044 (4)	1.4 ± 0.37 (5)

[a] Data taken from Ref. 18.
[b] Data taken from Ref. 17.

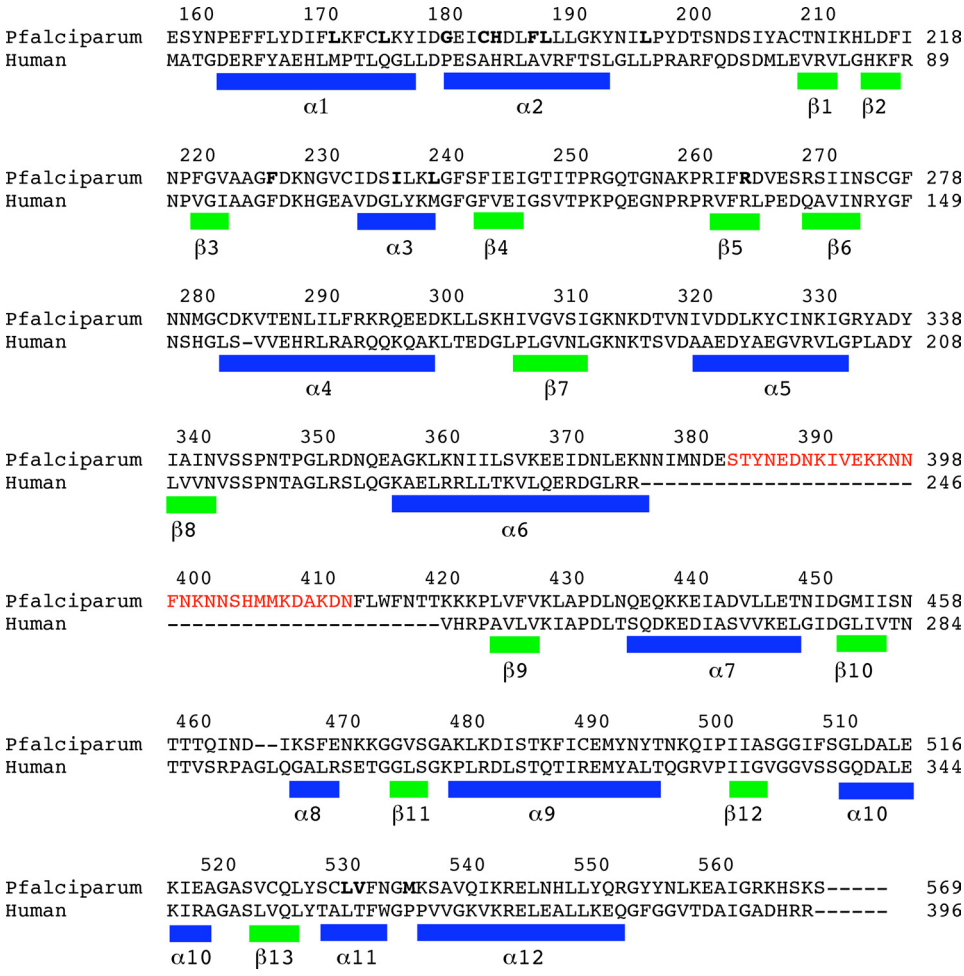

FIGURE 2. **Sequence alignment of *P. falciparum* and human DHODH.** Secondary structure elements are defined based on the *Pf*DHODH-DSM1 structure: α-helices are indicated by *blue bars*, and β-strands are indicated by *green bars*. Residues within 4 Å of DSM1 are displayed in *bold type*. The truncated surface loop in the *Pf*DHODH$\Delta_{384-413}$ construct used for structure determination is shown in *red*.

The three-dimensional fold of *Pf*DHODH in all three inhibitor bound complexes is similar to the previously reported structures of *Pf*DHODH bound to A77 1726 (14) and of human DHODH (*h*DHODH) (15). The enzyme consists of a short N-terminal helical domain (residues 163–194) followed by a classic β/α barrel domain that begins with β-strand 3 (Fig. 2 and 3*A*). The electron density maps of the active sites of all three structures showed strong, interpretable density for the bound inhibitors (DSM1, DSM2, or DSM74) (supplemental Fig. S1).

Triazolopyrimidine-binding Site—The inhibitor-binding site is formed adjacent to the FMN site between the two N-terminal helices (α1 and α2), the top of helix α3 in the β/α barrel, the 3_{10} helix α11, and strand β5 (Fig. 3*A*). The naphthyl of DSM1 interacts with α3, whereas the triazolopyrimidine group lies against α11. DSM1, DSM2, and DSM74 bind in the same site. The inhibitors are oriented such that the C-5 position of the triazolopyrimidine ring is the closest atom to FMN at a distance of 6 Å (Fig. 3). The inhibitors are bound in an extended conformation with the naphthyl (DSM1), anthracenyl (DSM2), or phenyl-trifluoromethyl (DSM74) groups oriented away from the triazolopyrimidine core and from FMN. The triazolopyrimidine ring in all three structures binds to a largely hydrophobic pocket formed by Val^{532}, Leu^{172}, Leu^{176}, Cys^{184}, and Gly^{181} (Fig. 3*B* and supplemental Fig. S2) that also contains two residues that form the only nonhydrophobic contacts in this pocket. These nonhydrophobic contacts include ion pair H-bonds between His^{185} and the bridging nitrogen N-1 and between Arg^{265} and the pyridine nitrogen N-5 (Fig. 4, *A* and *B*). We have defined this pocket as the H-bond pocket (Fig. 4*C*). The naphthyl (DSM1), anthracenyl (DSM2), or phenyl-trifluoromethyl (DSM74) groups bind in a completely hydrophobic pocket formed by residues Ile^{237}, Leu^{189}, Leu^{197}, Met^{536}, Phe^{227}, and Phe^{188} (Fig. 3*B* and supplemental Fig. S2), which we will define as the *Pf*naphthyl pocket (Fig. 4*C*). An edge-to-face stacking interaction between Phe^{227}, the aromatic group bound in the *Pf*naphthyl pocket, and Phe^{188}, is present (Fig. 4*A*), suggesting that these interactions likely contribute to the potent binding of the inhibitor series. These interactions involve the inhibitor in an extended aromatic stacking network that projects from FMN through Tyr^{528} to Phe^{227} on one face of the inhibitor and from Phe^{188} to Phe^{171} and beyond on the other side.

The van der Waal's surface of the DSM1-binding pocket shows that the inhibitor is buried in the interior

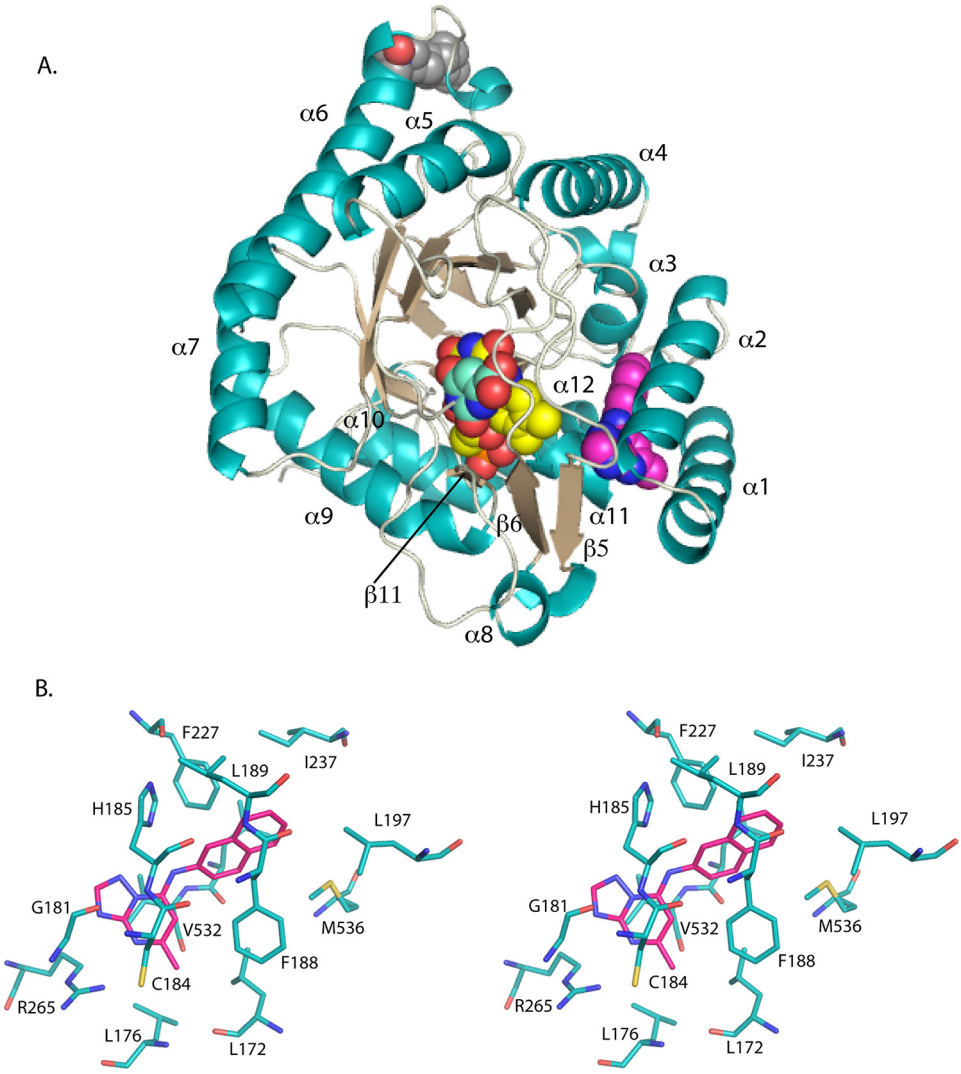

FIGURE 3. *A*, ribbon diagram of DSM1 bound to *Pf*DHODH. α-Helices are displayed in *teal*, β-strands are displayed in *sand*, ligands are displayed as space filling balls with FMN in *yellow*, DSM1 is in *pink*, orotate is in *turquoise*, and the bound detergent molecule is in *gray*. The position of the detergent corresponds to the position of the shortened surface loop truncated in the *Pf*DHODHΔ$_{384-413}$ construct. *B*, stereo diagram of the DSM1-binding site. Residues within 4 Å of the bound inhibitor are displayed. DSM1 is displayed in *pink*, and residues are displayed in *teal*. Nitrogen is displayed in *blue*, oxygen is in *red*, and sulfur is in *yellow*.

of the protein (Fig. 4*B*). The naphthyl is bound snuggly within a dead end hydrophobic pocket and the triazolopyrimidine ring, and the methyl side chain at C-6 also fit in close contact with the protein. A narrow channel leads from C-5 of the triazolopyrimidine ring toward FMN. An ordered water molecule (Wat^{15}) in this channel is observed in all three structures forming an H-bond with N-3 of the inhibitor and with the hydroxyl of Tyr^{528}, which in turn stacks against the FMN cofactor (Fig. 4*A*). This channel then extends from the FMN to the protein surface providing the only access to solvent for the bound ligands (FMN, orotate, and inhibitor). However, this channel is too narrow to allow passage of either substrate or inhibitor, and thus significant structural movement must accompany ligand binding.

Mutagenesis of Inhibitor-binding Pocket—The contribution to binding affinity of residues involved in H-bond (His^{185} and Arg^{265}) or π-stacking interactions (Phe^{227} and Phe^{188}) (Figs. 3 and 4 and supplemental Fig. S2) were probed by site-directed mutagenesis. We previously published the effects of mutating these four residues to Ala and demonstrated that these mutations had only minimal effects on catalytic activity (k_{cat} and K_m remain within 2–4-fold of the wild-type enzyme) (19). In contrast, mutation of each of these residues to Ala increased the IC$_{50}$ for DSM1 by 30–50-fold, demonstrating that each residue contributes significant binding energy to the enzyme inhibitor interaction (Table 1). The relative contribution of the mutated residues differs for the three inhibitors described in this study. For DSM2, the contribution of His^{185} and Arg^{265} is similar to DSM1; however Phe^{188} appears to play a reduced role in binding of this inhibitor. For DSM74, the H-bonds/ion pairs between His^{185} and Arg^{265} and inhibitor contribute more energy to the binding interaction than Phe^{188}. The IC$_{50}$ is increased by 80–90-fold for mutation of His^{185} and Arg^{265}, but only by 5-fold upon mutation of Phe^{188}. We previously analyzed only the F227A and R265A mutant enzymes against DSM1 (18); the IC$_{50}$ reported for R265A was similar to the value reported here in Table 1. However, the previously measured IC$_{50}$ for F227A was 30-fold higher; solubility problems may have contributed to this elevated value.

Small Molecule Structures of DSM Derivatives—Complementary insight into the importance of N-1 in the bridge position came from small molecule crystal structures of DSM1 and DSM74 in comparison with DSM1 analogs that contained an S (DSM15) or O (DSM16) in place of N-1 (Fig. 5, supplemental Figs. S3 and S4, and supplemental Tables S3–S5). DSM15 and DSM16 were tested against *Pf*DHODH, and they showed no inhibitory activity; thus the substitution of a single atom at the bridging position can eliminate binding. The small molecule x-ray structures of DSM1 and DSM74 show partial double-bond character of the C-1–N-1 bond connecting the bridging nitrogen to the triazolopyrimidine ring with observed C-1–N-1 bond lengths of 1.313 ± 0.006 and 1.344 ± 0.004 Å, respectively (supplemental Table S5) (typical C–N or C=N bond lengths are 1.38 and 1.28 Å, respectively (41)). In contrast, for analogs containing a bridging S (DSM15) or O (DSM16) in place of N-1, the C-1–S-1 and C-1–O-1 bond lengths were 1.740 ± 0.004 and 1.338 ± 0.003 Å, respectively, typical of single bonds (*e.g.* C–S/C–O bond lengths are 1.75/1.34 Å (27), whereas C=S/C=O bond lengths are 1.67/1.21 Å

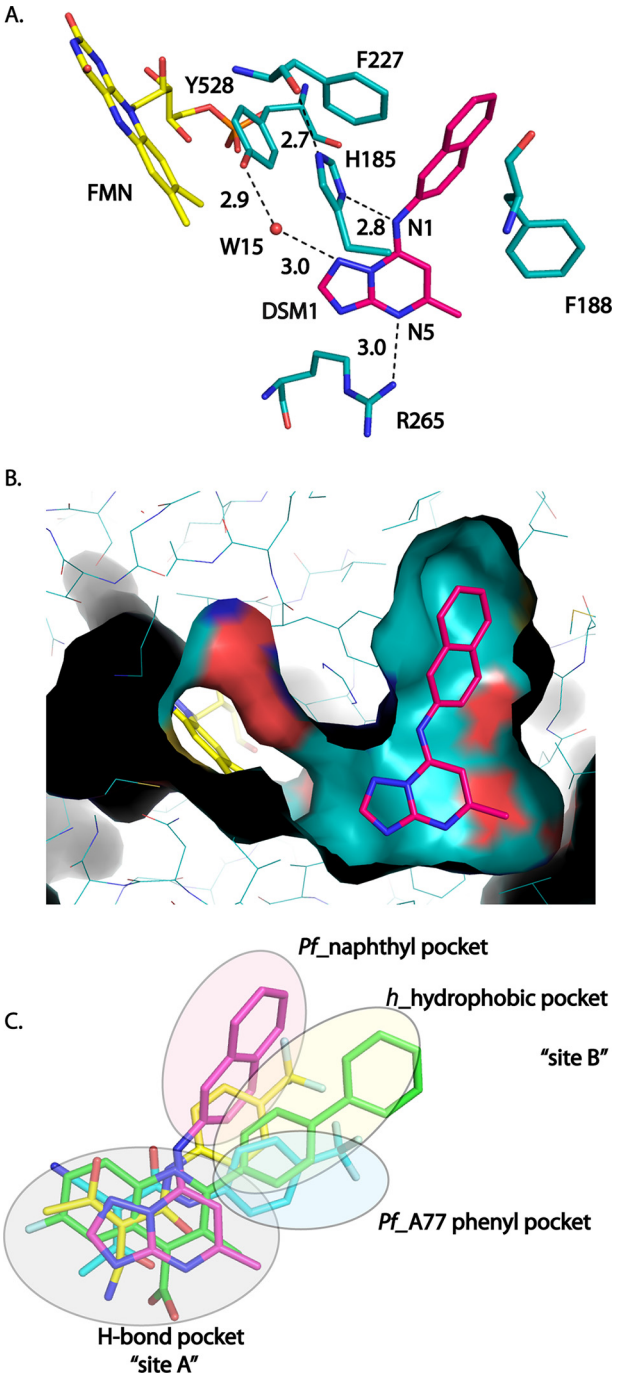

FIGURE 4. **DHODH inhibitor-binding site interactions.** *A*, H-bonding interactions between DSM1 and *Pf*DHODH. DSM1 is displayed in *pink*, and residues are displayed in *teal*. Distances are shown for H-bond interactions observed between the inhibitor and residues in the binding site. *B*, van der Waal's surface representation of DSM1 bound to *Pf*DHODH (*cyan*) as calculated by PyMol. Ligands were removed from the structure prior to calculation of the surface. The figure shows a narrow channel is present extending from C-5 of DSM1 to FMN. DSM1 is displayed in *pink*, FMN is displayed in *yellow*, and amino acid residues and the surface are displayed in *teal*. *C*, structural alignment of *Pf*DHODH and *h*DHODH inhibitor binding modes. The structures of *Pf*DHODH-DSM1 (*pink*), *Pf*DHODH-A77 (*turquoise*), *h*DHODH-bre (*green*), and *h*DHODH-A77 (*yellow*) were superimposed as described in methods. Only the bound inhibitor is displayed.

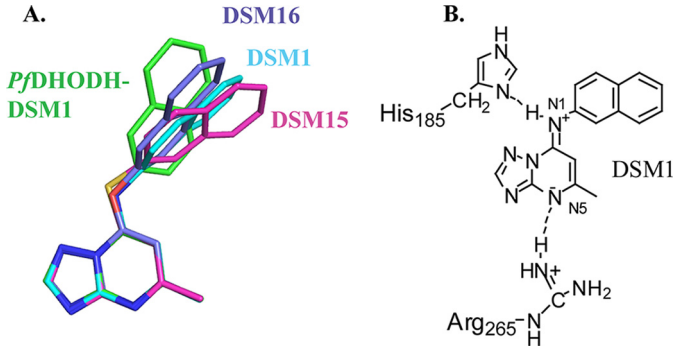

FIGURE 5. **Comparison of protein bound inhibitor conformations with free ligand structures.** *A*, comparison of the conformation of DSM1 bound to *Pf*DHODH (*green*) with the conformations of DSM1 (*cyan*), DSM15 (*pink*), and DSM16 (*purple*) as observed in the small molecule x-ray structures. *B*, schematic resonance structure of DSM1 forming H-bonding ion pair interactions with *Pf*DHODH. H-bonds are depicted by the *dashed line*.

(41), respectively). Additionally, partial positive charge character of N-1 is further suggested by hydrogen bonding to a chloride ion in the DSM1 structure. These data suggest that when the bridging atom is N-1, resonance contributes to greater electron delocalization to N-5, intrinsically establishing long range dipoles in the inhibitor. In the protein, electron delocalization of the inhibitor is exploited by the H-bond with His^{185}, which results in sufficient electron density on N-5 to allow formation of an ion pair with Arg^{265} (Figs. 4*A* and 5*B*). Such electron delocalization is more limited, or absent, for molecules containing O or S in the bridging position, providing an explanation for their inactivity as *Pf*DHODH inhibitors. Thus the intrinsic dipole of the triazolopyrimidine ring is a key factor in the potency of this compound class toward *Pf*DHODH.

Not all aspects of the small molecule conformation translate to what is observed on the protein. The plane of the naphthyl group in the protein-bound state is twisted by 48° relative to its unbound conformation (Fig. 5*A*). This conformational difference is necessary to position the naphthyl group of DSM1 to interact productively with the enzyme.

Plasticity to Accommodate Different Sized Triazolopyrimidine Inhibitors—Globally, the DSM1, DSM2, and DSM74-bound *Pf*DHODH structures are very similar with RMSD for superimposition of the C_α atoms of ~0.4 Å among them (Figs. 6*A*). The inhibitors occupy very similar positions in all three structures. The different size N-1 substituents are accommodated by conformational flexibility in the binding pocket. In both the *Pf*DHODH-DSM2 and *Pf*DHODH-DSM74 structures the triazolopyrimidine ring tilts slightly toward the bottom of the H-bond pocket relative to *Pf*DHODH-DSM1. Leu^{176} reorients to accommodate this change. Further for *Pf*DHODH-DSM74, this slight shift (0.2 Å) brings Ile^{263} into van der Waal's contact with the C-5 position of the inhibitor. For *Pf*DHODH-DSM2, the anthracenyl extends further into the binding site than naphthyl of DSM1. The larger aromatic group is accommodated by small rotational changes in Leu^{197} and Met^{536} that enlarge the *Pf*naphthyl pocket. New contacts are also made with Leu^{240} and Cys^{233}. The smaller phenyl-trifluoromethyl group of DSM74 does not completely fill the pocket and makes fewer van der Waal's contacts. In particular Ile^{237} and Leu^{189} are no longer within the 4 Å van der Waal's shell of DSM74. However, a new contact is made between the CF_3 group and Leu^{240} in this structure. The reduced surface area of contact likely explains why DSM74 is 10-fold less potent than DSM1 or DSM2.

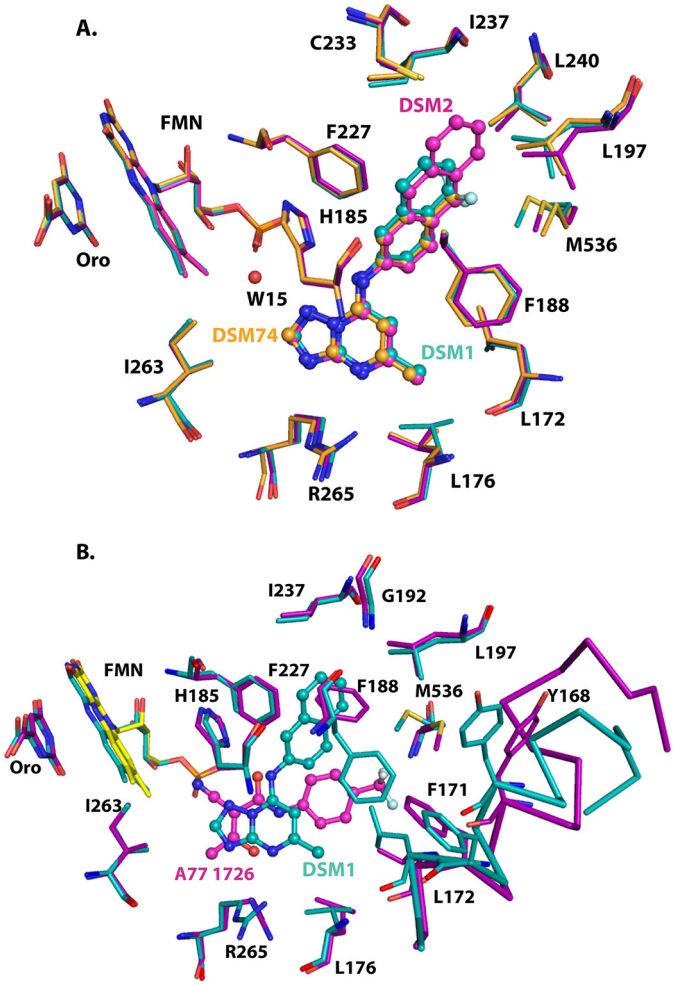

FIGURE 6. **Comparison of *Pf*DHODH inhibitor complexes.** *A*, *Pf*DHODH-DSM1 (*teal*) superimposed with *Pf*DHODH-DSM2 (*purple*) and with *Pf*DHODH-DSM74 (*orange*). *B*, *Pf*DHODH-DSM1 (*teal*) superimposed with *Pf*DHODH-A77 (*purple*). A subset of residues within 4 Å of the bound inhibitor are displayed. FMN (*yellow*) and orotate (*Oro*), which are outside this shell, are included to provide orientation. Inhibitors are displayed as ball and stick.

Conformational Flexibility of PfDHODH Accounts for Binding to Diverse Chemical Scaffolds—Comparison of the *Pf*DHODH-DSM1 with *Pf*DHODH-A77 structures shows that *Pf*DHODH can present two alternative binding sites for interactions with different inhibitor classes. The *Pf*DHODH-DSM1 and *Pf*DHODH-A77 structures superimpose with a C_α RMSD of 1.03 Å, much larger than the 0.4 Å RMSD observed between the three triazolopyrimidine class inhibitors. Both inhibitors occupy the H-bond pocket such the triazolopyrimidine ring and the β-hydroxy enamide portion of A77 1726 overlap in this site (Figs. 4*C* and 6*B*). In contrast, the aromatic N-1 substituent in the triazolopyrimidines binds in an entirely different position from the phenyl-trifluoromethyl of A77 1726. These different binding modes are created by a large conformational change in the position of Phe^{188} between the two structures. In *Pf*DHODH-A77, Phe^{188} occupies the *Pf*naphthyl pocket, and in the *Pf*DHODH-DSM1 Phe^{188} rotates to overlap the position of the phenyl-trifluoromethyl in *Pf*DHODH-A77 (defined as the *Pf*A77 phenyl pocket; Fig. 4*C*). In addition, Met^{536}, Cys^{175}, Leu^{176}, and residues on helix α1 (Tyr^{168}, Asp^{169}, Phe^{171}, and Leu^{172}) show conformational flexibility between the two structural classes of inhibitors. Further, helix α1 shifts toward the interior of the protein in *Pf*DHODH-DSM1, further restricting the *Pf*A77 phenyl pocket. Similar structural differences are observed between *Pf*DHODH-A77 and *Pf*DHODH-DSM2 and *Pf*DHODH-DSM74.

Host-Parasite Differences—To understand the species-selective binding of the various inhibitor classes, *Pf*DHODH bound to the triazolopyrimidines was compared with *h*DHODH in complex with brequinar and A77 1726 (Fig. 7). Alignment of the C_α backbone of *Pf*DHODH-DSM1 with *h*DHODH-bre or with *h*DHODH-A77 gave an overall RMSD of 1.8 or 1.9 Å, respectively. Brequinar, which is a potent inhibitor of *h*DHODH, forms some analogous interactions to the triazolopyrimidine core of DSM1 (Fig. 7, *A* and *B*). The 4-quinolinecarboxylic acid of brequinar binds the same site (H-bond pocket) as the triazolopyrimidine ring, forming a salt bridge between the carboxylate and *h*Arg^{136} (equivalent to *P. falciparum* Arg^{265} interacting with N-5 of DSM1). This interaction is thought to play a major role in driving binding affinity (15, 42). In contrast, the biphenyl portion of brequinar binds to a distinct and different hydrophobic site (defined as the *h*_hydrophobic pocket) from the naphthyl-group of DSM1, which binds *Pf*DHODH at the adjacent malaria-specific site (*Pf*naphthyl pocket). The *h*_hydrophobic pocket lies between the DSM1 *Pf*naphthyl pocket and the *Pf*A77 phenyl pocket of A77 1726 when bound to *Pf*DHODH (Fig. 4*C*).

These sites represent alternative pockets that are species-specific and are created by the different amino acid composition of the pockets (Fig. 7, *A* and *B*). The *h*_hydrophobic pocket that binds the brequinar biphenyl group is occluded in *Pf*DHODH by replacement of the smaller *h*Ala^{59} and *h*Pro^{364} in *h*DHODH with the larger *Pf*Phe^{188} and *Pf*Met^{536} residues in *Pf*DHODH and by the repositioning of *Pf*Tyr^{168} (*h*Tyr^{38}) closer to the inhibitor-binding pocket by the movement of the N-terminal α1 helix. Additionally *h*Leu^{68} is positioned further from the biphenyl pocket than the equivalent residue *Pf*Leu^{197} in *Pf*DHODH. On the flip side, in *Pf*DHODH the naphthyl pocket is opened up relative to *h*DHODH by the replacement of *h*Thr^{63} and *h*Met^{111} with *Pf*Gly^{192} and *Pf*Leu^{240}. Further the positions of *Pf*Phe^{227} and *Pf*Leu^{531} relative to the equivalent residues in *h*DHODH (*h*Phe^{98} and *h*Leu^{359}) have swung away from the naphthyl position in *Pf*DHODH-DSM1, enlarging the pocket relative to *h*DHODH. Globally the N-terminal helix (Ser^{160} to Tyr^{178}) in *Pf*DHODH is packed more closely to the inhibitor-binding site than the analogous helix (residues Met^{30} to Gly^{48}) in *h*DHODH (Fig. 7*A*). This difference contributes to closing of the *h*_hydrophobic pocket in *Pf*DHODH.

A77 1726 is smaller than brequinar and does not extend as deeply into the *h*_hydrophobic pocket (Fig. 7*C*). Furthermore, the phenyl-trifluoromethyl group binds slightly closer to the *Pf*naphthyl pocket then brequinar. The β-hydroxy enamide portion of A77 1726 is flipped over in the *h*DHODH structure relative to when bound to *Pf*DHODH. This changes the angle of projection of the phenyl-trifluoromethyl group into the hydrophobic pocket, allowing it to access the *h*_hydrophobic pocket instead of the *Pf*A77 phenyl pocket. Similar residues contribute to the differential binding as was observed for brequinar. Again the replacement of *h*Ala^{59} with *Pf*Phe^{188} and *h*Pro^{364} with

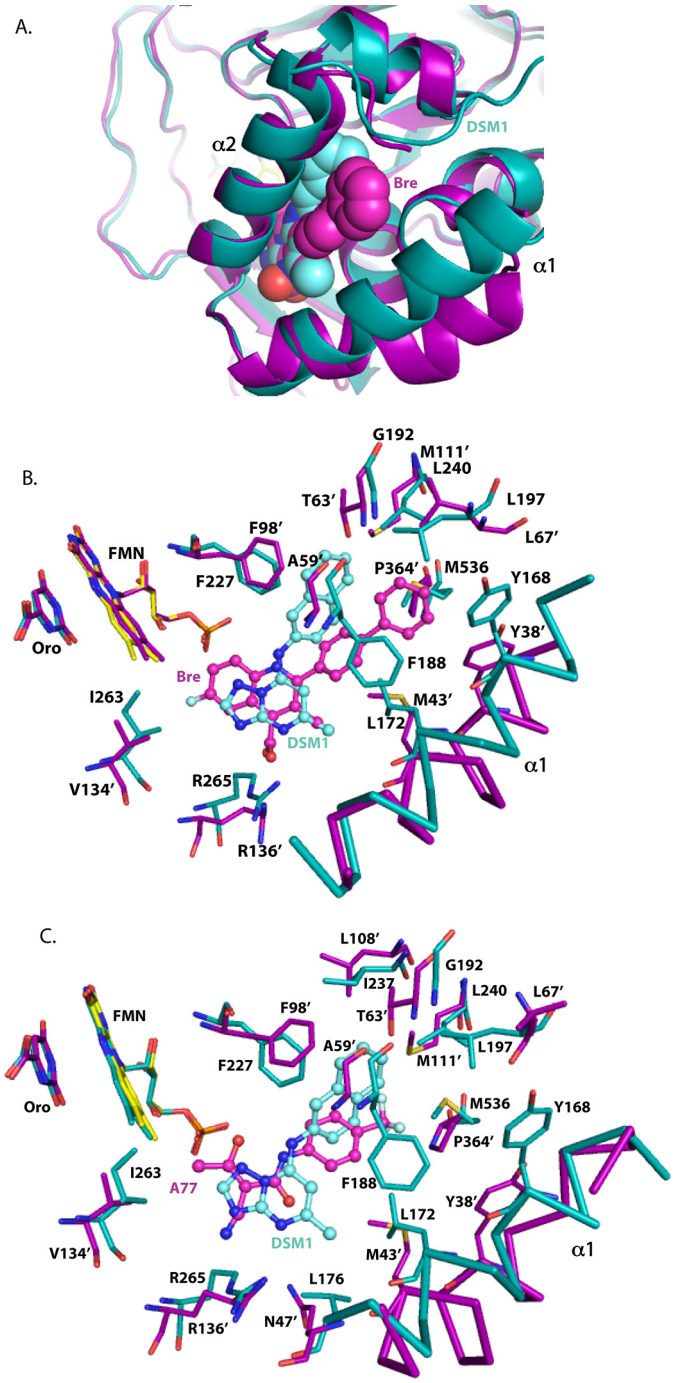

FIGURE 7. **Comparison of *Pf*DHODH-DSM1 to *h*DHODH inhibitor complexes.** *A*, ribbon diagram of *Pf*DHODH-DSM1 (*teal*) aligned with *h*DHODH-bre (*purple*). Inhibitors are displayed as space filling balls. *B*, inhibitor-binding site alignment of *Pf*DHODH-DSM1 (*teal*) with *h*DHODH-bre (*purple*). *C*, inhibitor-binding site alignment of *Pf*DHODH-DSM1 (*teal*) with *h*DHODH-A77 (*purple*). Residue numbers for *h*DHODH are marked with a prime symbol, whereas *Pf*DHODH numbers are not. Inhibitors are displayed as ball and stick.

*Pf*Met^{536} closes off the phenyl-trifluoromethyl pocket of A77 1726 in *Pf*DHODH relative to the *h*DHODH structure.

DISCUSSION

Malaria remains one of the most significant global health problems because of wide spread drug resistance compromising current chemotherapies. One of the greatest challenges in developing new anti-malarial agents is the identification of novel targets that will allow the discovery of unexplored chemical scaffolds. Our discovery of the triazolopyrimidine-based inhibitors of *Pf*DHODH has led to the validation of *Pf*DHODH as a target for the development of new anti-malarials and to the identification of a novel chemical class with *in vivo* anti-malarial activity (17, 18). Here we report the x-ray structures of *Pf*DHODH bound to three triazolopyrimidine-based inhibitors. First, these data show that structural plasticity allows the triazolopyrimidine-based inhibitors to access an unexpected hydrophobic binding pocket that was not observed in previous structures. This structural flexibility allows the target to accommodate a range of inhibitors from different structural classes. A second unexpected insight was gained by comparison of the small molecule x-ray structures of the inhibitors with the protein-bound ligand structures. The intrinsic electronic configuration of the triazolopyrimidine ring favors charge delocalization from N-1 to N-5, providing significant insight into the emerging SAR of the triazolopyrimidine-based series. Finally, the variability in amino acid sequence between the human and malaria DHODH inhibitor-binding sites leads to species-selective inhibitor binding modes that explain the selectivity of the triazolopyrimidine-based inhibitors.

The malaria enzyme has the flexibility to form two different inhibitor-binding pockets (*Pf*naphthyl pocket and the *Pf*A77 phenyl pocket). This flexibility is likely to underlie the finding that multiple inhibitor series have been reported for *Pf*DHODH that sample diverse chemical space (17, 18, 21–24). Although the triazolopyrimidine derivatives interact with the *Pf*naphthyl pocket, other identified inhibitors are likely to bind to the *Pf*A77 phenyl pocket, explaining how the enzyme can accommodate these wide ranging scaffolds. Additionally local flexibility within the *Pf*naphthyl pocket contributes to the ability of this pocket to bind ligands of variable size. Flexibility in inhibitor binding modes has also been observed in *h*DHODH associated with conformational changes in the position of *h*Arg^{136} and *h*Gln^{47} (42), the N-terminal helix (α1) (11) and a loop (*h*Leu^{68}–*h*Arg^{72}) postulated to perform a gate keeper function (43). Thus structural plasticity appears to be an inherent property of the DHODH enzyme family, enhancing the suitability of this enzyme as a drug target by creating many design options and reducing the risks or liabilities that would be associated with only a single chemical class. Additionally the ability of the enzyme to adapt to different analogs within a structural class provides sites for modification during lead optimization to improve pharmacological properties. Protein flexibility has been observed in a wide array of known drug targets (44–46), and protein dynamics is increasingly being incorporated into drug design strategies (47–51). Thus structural plasticity leading to binding of diverse inhibitor classes can be appreciated as an important property of high value drug targets guiding future target selection for drug discovery projects.

Analysis of drug interactions that are involved in conformational changes in the target protein suggests that hydrophobic inhibitors can induce refolding of local regions of the binding pocket leading to high affinity interactions (46). This suggests that the triazolopyrimidine-based inhibitors induce a refolding of the aromatic network by reorienting Phe^{188} and allowing the

naphthyl-functionality to insert into an extended edge-to-face stacking network that runs through the protein. Alternatively the inhibitors may selectively bind and stabilize a pre-existing conformation of the aromatic network that is part of the native state ensemble but that has not previously been observed. Aromatic edge-to-face stacking interactions provide additional binding energy beyond a typical van der Waal's contact (52) as has been observed previously for potent binding of carboxypeptidase inhibitors (53). Our data support a role for these interactions in inhibitor binding to *Pf*DHODH because mutation of residues in this network (Phe^{227} and Phe^{188}) resulted in a significant reduction in binding affinity.

The intrinsic electronic properties of the triazolopyrimidine ring allow it to populate a resonance form that promotes charge separation, which is key to the formation of H-bond interactions with the enzyme. The importance of these ion pair interactions to inhibitor potency is supported both by the site-directed mutagenesis data and by the chemical modification of the inhibitor. When N-1 is replaced with atoms that are unable to delocalize electrons into the triazolopyrimidine ring (S or O), the IC_{50} increases by >4.4 kcal/mol. Interestingly mutation of His^{185} or Arg^{265} each reduced the binding affinity by 2–3 kcal/mol, suggesting that if the contributions of these two residues are additive, the loss in binding energy by replacing the bridging nitrogen with S or O is equivalent to losing both interactions.

The x-ray structures of *Pf*DHODH bound to the triazolopyrimidine-based inhibitors represent the first structural studies of the malarial enzyme bound to malaria-specific inhibitors, and as such they provide considerable new insight into species selective binding in this enzyme family. The inhibitor-binding pocket can be divided into site A (the H-bond pocket), which forms H-bonding interactions with the bound inhibitors, and site B, which is entirely hydrophobic (Fig. 4*C*). Both malaria and human-specific inhibitors interact with site A. Species selectivity of inhibitor binding arises from differences in the orientation of site B relative to site A within the protein structure. These differences have their basis in the species-specific amino acid composition of the inhibitor-binding pockets. For the triazolopyrimidine analogs, specificity for *Pf*DHODH arises from the projection of an aromatic side chain from the N-1 position into the *Pf*naphthyl pocket, which is blocked in the human structure. Whereas for brequinar the presence of the biphenyl group on the equivalent position to C-2 of DSM1 allows good interaction with the *h*_hydrophobic pocket, this orientation cannot be accommodated by either the site B-binding pocket on *Pf*DHODH. The structural basis for differential binding of A77 1726 is similar. The fact that residues that form H-bonds with the triazolopyrimidine ring (*Pf*His^{185} and *Pf*Arg^{265}) are conserved in the human enzyme suggests inhibitors of *h*DHODH could also be developed based on this core scaffold.

The x-ray structures of *Pf*DHODH bound to the triazolopyrimdine inhibitors provide significant insight into the observed SAR for this series. In addition to explaining the loss of activity upon replacing the bridging nitrogen N-1 with S or O, several other aspects of the SAR (17, 18) can now be readily understood. First we have observed that when the aromatic group is a phenyl, para substitutions yield good binding potency, whereas ortho substitutions are completely inactive. The *Pf*DHODH-DSM74 structure shows that the ortho carbon atoms are 4.1 Å from the carbonyl oxygen of His^{185} on one side and 4.0Å from the CD1 of Leu^{172} on the other. Thus based on the current structures there is not space in the pocket to accommodate ortho substituents, nor apparently is this region of the binding pocket capable of the conformational flexibility that would be needed to accommodate this substitution. Second, the completely hydrophobic nature of the *Pf*naphthyl pocket explains why aromatic rings containing heteroatoms show reduced potency. Third, the close interaction between His^{185} and the bridging nitrogen N-1 explains why a secondary nitrogen is required at this position and why the addition of a third substituent on the nitrogen reduces potency. Finally, the potential for stacking interactions between Phe^{227} and Phe^{188}, in addition to the hydrophobic nature of the pocket, explains why large aromatic groups are favored.

In summary, x-ray structure determination of *Pf*DHODH in complex to three triazolopyrimidine-based inhibitors has provided insight into the structural basis for potent and species-selective binding of this series of inhibitors. It has advanced our understanding of the emerging SAR for this promising lead series. Ongoing efforts to improve the potency and *in vivo* properties of the triazolopyrimidine-lead series will be greatly aided by these studies. More broadly, the results have provided insight into the structural requirements for designing species-selective inhibitors of either malarial or human DHODH that can be applied to scaffolds beyond the triazolopyrimidine analogs. Finally, the advantages of attacking plastic active sites in lead optimization offer general lessons for prioritizing structure-based protein-ligand interactions for pharmaceutical applications.

Acknowledgments—We thank Diana Tomchick and Mischa Machius of the University of Texas Southwestern crystallography core for help with data collection and David Matthews and Jeremy Burrows for insightful and helpful discussions.

REFERENCES

1. Greenwood, B. M., Fidock, D. A., Kyle, D. E., Kappe, S. H., Alonso, P. L., Collins, F. H., and Duffy, P. E. (2008) *J. Clin. Invest.* **118,** 1266–1276
2. Guerra, C. A., Gikandi, P. W., Tatem, A. J., Noor, A. M., Smith, D. L., Hay, S. I., and Snow, R. W. (2008) *PLoS Med.* **5,** e38
3. White, N. J. (2004) *J. Clin. Invest.* **113,** 1084–1092
4. Rosenthal, P. J. (2008) *N. Engl. J. Med.* **358,** 1829–1836
5. Gutteridge, W. E., and Trigg, P. I. (1970) *J. Protozool.* **17,** 89–96
6. Reyes, P., Rathod, P. K., Sanchez, D. J., Mrema, J. E., Rieckmann, K. H., and Heidrich, H. G. (1982) *Mol. Biochem. Parasitol.* **5,** 275–290
7. Jones, M. E. (1980) *Annu. Rev. Biochem.* **49,** 253–279
8. Nagy, M., Lacroute, F., and Thomas, D. (1992) *Proc. Natl. Acad. Sci. U.S.A.* **89,** 8966–8970
9. Painter, H. J., Morrisey, J. M., Mather, M. W., and Vaidya, A. B. (2007) *Nature* **446,** 88–91
10. Goldenberg, M. M. (1999) *Clin. Ther.* **21,** 1837–1852
11. Olsen, N. J., and Stein, C. M. (2004) *N. Engl. J. Med.* **350,** 2167–2179
12. Baldwin, J., Farajallah, A. M., Malmquist, N. A., Rathod, P. K., and Phillips, M. A. (2002) *J. Biol. Chem.* **277,** 41827–41834
13. Copeland, R. A., Marcinkeviciene, J., Haque, T. S., Kopcho, L. M., Jiang, W., Wang, K., Ecret, L. D., Sizemore, C., Amsler, K. A., Foster, L., Tadesse, S., Combs, A. P., Stern, A. M., Trainor, G. L., Slee, A., Rogers, M. J., and Hobbs, F. (2000) *J. Biol. Chem.* **275,** 33373–33378
14. Hurt, D. E., Widom, J., and Clardy, J. (2006) *Acta Crystallogr. D Biol.*

Crystallogr. **62,** 312–323
15. Liu, S., Neidhardt, E. A., Grossman, T. H., Ocain, T., and Clardy, J. (2000) *Structure* **8,** 25–33
16. Baldwin, J., Michnoff, C. H., Malmquist, N. A., White, J., Roth, M. G., Rathod, P. K., and Phillips, M. A. (2005) *J. Biol. Chem.* **280,** 21847–21853
17. Gujjar, R., Marwaha, A., El Mazouni, F., White, J., White, K. L., Creason, S., Shackleford, D. M., Baldwin, J., Charman, W. N., Buckner, F. S., Charman, S., Rathod, P. K., and Phillips, M. A. (2009) *J. Med. Chem.* **52,** 1864–1872
18. Phillips, M. A., Gujjar, R., Malmquist, N. A., White, J., El Mazouni, F., Baldwin, J., and Rathod, P. K. (2008) *J. Med. Chem.* **51,** 3649–3653
19. Malmquist, N. A., Gujjar, R., Rathod, P. K., and Phillips, M. A. (2008) *Biochemistry* **47,** 2466–2475
20. Srivastava, I. K., Morrisey, J. M., Darrouzet, E., Daldal, F., and Vaidya, A. B. (1999) *Mol. Microbiol.* **33,** 704–711
21. Boa, A. N., Canavan, S. P., Hirst, P. R., Ramsey, C., Stead, A. M., and McConkey, G. A. (2005) *Bioorg. Med. Chem.* **13,** 1945–1967
22. Heikkilä, T., Ramsey, C., Davies, M., Galtier, C., Stead, A. M., Johnson, A. P., Fishwick, C. W., Boa, A. N., and McConkey, G. A. (2007) *J. Med. Chem.* **50,** 186–191
23. Heikkilä, T., Thirumalairajan, S., Davies, M., Parsons, M. R., McConkey, A. G., Fishwick, C. W., and Johnson, A. P. (2006) *Bioorg. Med. Chem. Lett* **16,** 88–92
24. Patel, V., Booker, M., Kramer, M., Ross, L., Celatka, C. A., Kennedy, L. M., Dvorin, J. D., Duraisingh, M. T., Sliz, P., Wirth, D. F., and Clardy, J. (2008) *J. Biol. Chem.* **283,** 35078–35085
25. Lakaschus, G., and Löffler, M. (1992) *Biochem. Pharmacol.* **43,** 1025–1030
26. DeLano, W. L. *The Pymol Molecular Graphics System* (2000) DeLano Scientific, San Carlos, CA
27. Otwinowski, Z., and Minor, W. (1997) *Methods Enzymol.* **276,** 307–326
28. McCoy, A. J. (2007) *Acta Crystallogr.* **63,** 32–41
29. Emsley, P., and Cowtan, K. (2004) *Acta Crystallogr.* **60,** 2126–2132
30. Murshudov, G. N., Vagin, A. A., and Dodson, E. J. (1997) *Acta Crystallogr.* **53,** 240–255
31. Cowtan, K. (1998) *Acta Crystallogr.* **54,** 750–756
32. Kleywegt, G. J., and Jones, T. A. (1994) *CCP4/ESF-EACBM Newsletter on Protein Crystallography* **31,** 9–14
33. Kabsch, W., Kabsch, H., and Eisenberg, D. (1976) *J. Mol. Biol.* **100,** 283–291
34. Kleywegt, G. J., and Jones, T. A. (1997) *Methods Enzymol.* **277,** 525–545
35. Kleywegt, G. J. (1999) *Acta Crystallogr. D Biol. Crystallogr.* **55,** 1878–1884
36. Altomare, A., Burla, C., Camalli, M., Cascarano, L., Giacovazzo, C., Guagliardi, A., Moliterni, A., Polidori, G., and Spagna, R. (1999) *J. Appl. Crystallogr.* **32,** 115–119
37. Sheldrick, G. (1997) *SHELXL97*, University of Gottingen, Gottingen, Germany
38. Waasmaier, D., and Kirfel, A. (1995) *Acta Crystallogr. A* **51,** 416
39. Flack, H. (1983) *Acta Crystallogr.* **A39,** 876–881
40. Farrugia, L. (1997) *Appl. Crystallogr.* **30,** 565
41. March, J. (2006) *Advanced Organic Chemistry: Reactions, Mechanisms, and Structure*, 4th ed., p. 21, Wiley India Pvt. Ltd.
42. Baumgartner, R., Walloschek, M., Kralik, M., Gotschlich, A., Tasler, S., Mies, J., and Leban, J. (2006) *J. Med. Chem.* **49,** 1239–1247
43. Walse, B., Dufe, V. T., Svensson, B., Fritzson, I., Dahlberg, L., Khairoullina, A., Wellmar, U., and Al-Karadaghi, S. (2008) *Biochemistry* **47,** 8929–8936
44. McCammon, J. A. (2005) *Biochim. Biophys. Acta* **1754,** 221–224
45. Hornak, V., and Simmerling, C. (2007) *Drug Discov. Today* **12,** 132–138
46. Teague, S. J. (2003) *Nat. Rev. Drug Discov.* **2,** 527–541
47. Amaro, R. E., Baron, R., and McCammon, J. A. (2008) *J. Comput. Aided Mol. Des.* **22,** 693–705
48. B-Rao, C., Subramanian, J., and Sharma, S. D. (2009) *Drug Discov. Today* **14,** 394–400
49. Bowman, A. L., Lerner, M. G., and Carlson, H. A. (2007) *J. Am. Chem. Soc.* **129,** 3634–3640
50. Chène, P. (2008) *Drug Discov. Today* **13,** 522–529
51. Crespo, A., and Fernández, A. (2008) *Mol. Pharm.* **5,** 430–437
52. Burley, S. K., and Petsko, G. A. (1985) *Science* **229,** 23–28
53. Kim, H., and Lipscomb, W. N. (1991) *Biochemistry* **30,** 8171–8180
54. Knecht, W., and Löffler, M. (1998) *Biochem. Pharmacol.* **56,** 1259–1264
55. Ullrich, A., Knecht, W., Fries, M., and Loffler, M. (2001) *Eur. J. Biochem./FEBS* **268,** 1861–1868
56. Copeland, R. A., Davis, J. P., Dowling, R. L., Lombardo, D., Murphy, K. B., and Patterson, T. A. (1995) *Arch. Biochem. Biophys.* **323,** 79–86